Growth of Long ZnO Nanowires with High Density on the ZnO Surface for Gas Sensors

Alex C. Campos,[†] Suane C. Paes,[†] Bruno S. Correa,[†] Gabriel A. Cabrera-Pasca,[†] Messias S. Costa,[†] Cleidilane S. Costa,[†] Larissa Otubo,[‡] and A. W. Carbonari*,[‡]

[†]Faculdade de Ciências Exatas e Tecnologia (FACET), Universidade Federal do Pará, Campus Universitário de Abaetetuba, 68.440-000 Abaetetuba, PA, Brazil

[‡]Instituto de Pesquisas Energéticas e Nucleares, IPEN, Universidade de São Paulo, 05508-000 São Paulo, SP, Brazil

ABSTRACT: Among the various approaches to grow semiconducting oxide nanowires, the thermal oxidation procedure is considered a simple, efficient, and fast method that allows the synthesis of micro and nanostructured arrangements with controlled size and morphology. In the work reported in this paper, long ZnO nanowires were synthesized on the surface of oxidized high-purity Zn foils by heating in air at different rates and temperatures. The size and morphology investigated by scanning electron microscopy (SEM) and high-resolution transmission electron microscopy (HRTEM) for a sample heated at 620 °C with heating rate of 20 °C/min reveal the growth of long ZnO nanowires with length of ∼50 μm and average diameter of 74 nm grown along

the ⟨11$\bar{2}$0⟩ direction with high population density. Results with different heating rates indicates that this parameter is determinant in tuning the size, morphology, and population density of nanowires. X-ray diffraction (XRD) shows patterns for both ZnO and metallic Zn with preferential orientation, whereas perturbed angular correlation (PAC) measurements using ^{111}In(^{111}Cd) probe nuclei indicate that probe nuclei occupy only Zn sites in the preferential oriented metallic zinc. However, for samples submitted to high-temperature heating (820 and 1000 °C), XRD yields only the ZnO pattern and, amazingly, PAC continues showing probe nuclei only at metallic Zn sites indicating the presence of thin regions of highly oriented Zn trapped between grains of ZnO. Moreover, this strong preference of indium atoms (of parent radioactive ^{111}In) here revealed helps to understand the oxidation mechanism and the growth of the nanowires.

KEYWORDS: *ZnO, nanowires, one-dimensional semiconducting oxides, oxidation, electric field gradient*
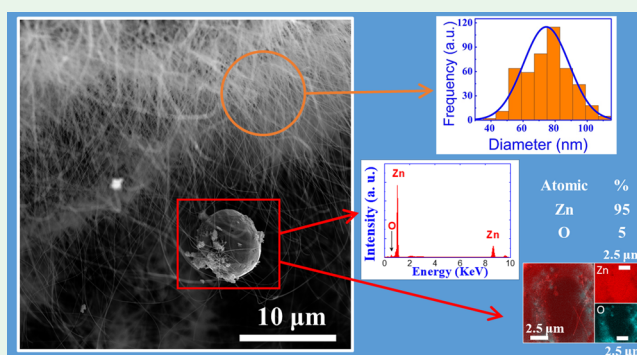
INTRODUCTION

ZnO nanowires are used for different applications such as gas sensors, nanogenerators and photocatalysis, optical emission, optoelectronic devices, piezoelectric transducers and actuators, and biosensors.[1−3] The growth of extended and oriented nanostructures composed of high density ZnO nanowires like long branched "treelike" and other complex nanostructures are desirable for photoanodes and many other applications, but it is still challenging to synthesize complex nanostructures with controlled crystalline morphology, orientation, and surface architecture.[4,5]

Nanowires, nanobelts, nanowhiskers, and hierarchical structures have been produced by using different physical and chemical routes in many experiments. Several of these materials are synthesized from metals (Au,Cu,Ag),[6,7] semiconductors (Si, Ge, GaAs, PbS),[8−11] and transition metal oxides (ZnO, CuO, Fe$_2$O$_3$),[12−15] each one having very interesting physical and chemical properties that can be used in the construction of miniaturized devices. In order to control the length, morphology, and doping in these one-dimensional materials, simple and elaborated experimental arrangements

have been developed, such as metalorganic chemical vapor deposition (MOCVD),[16,17] physical vapor deposition,[18] molecular beam epitaxy (MBE) flux methods,[9,10] pulsed laser deposition (PLD),[19] and thermal oxidation method.[12−15] Essentially, some of the striking effects observed on these low-dimensional structures are attributed to the increase in the atomic density on the surface of the nanostructure arrangements, which is not observed in macroscopic materials. Therefore, the ratio of the surface area to the volume is a good parameter to investigate the exotic chemical and physical properties of these low-dimensional structures.

Among the synthesis methods developed for synthesizing one-dimensional semiconductor oxides reported, the thermal oxidation has been highlighted because it has shown to be a simple, efficient, fast and low-cost technique for nanowire synthesis. In this method, the metal precursors are simply subjected to heat treatments at high temperatures. However,

Scheme 1. Thermal Oxidation Process of Zn Foils Which Results in the Formation of Long ZnO Nanowires on the ZnO Surface
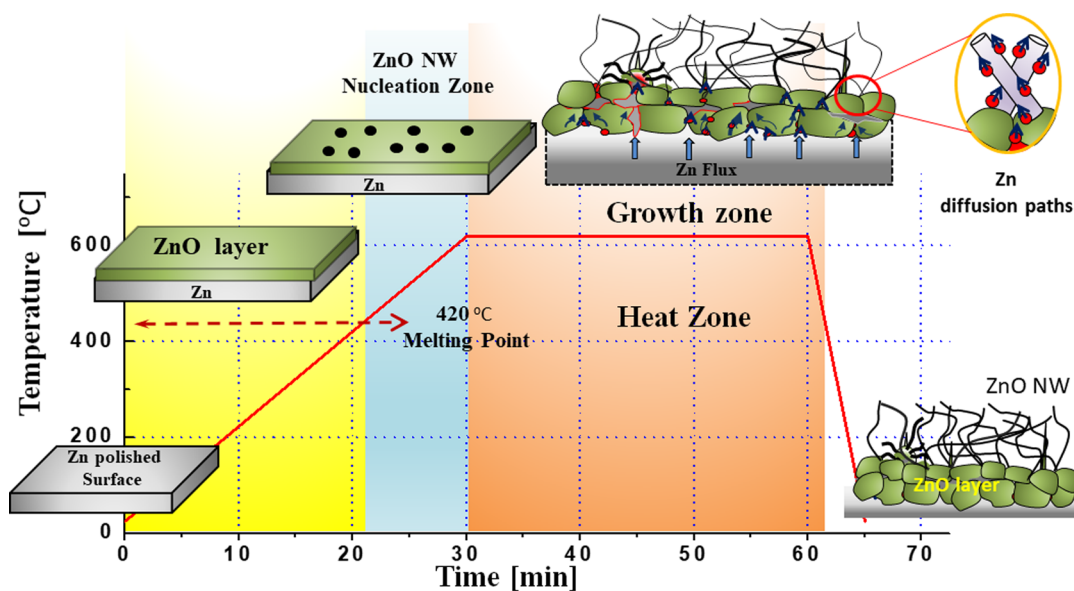
changes in size and morphology can be achieved by controlling the reaction atmosphere, heating rates, or introducing the passage of electric current through the wire during the synthesis process.[12−15]

Different mechanisms or driving forces are involved during the oxidation process and have been discussed by the scientific community in previous papers.[12−14,20−22] The performance of the thermal oxidation method to grow one-dimensional structures is very reliable; consequently, the characterization of samples obtained by this method has been used as a test for mathematical models developed to predict potential applications of nanowire structures. A good example is the work reported by Lin et al.,[23] which describes the application of CuO in field emission, where a mathematical model was tested using samples synthesized by thermal oxidation method, showing the degree of reliability of this simple method. Another interesting application of the thermal oxidation method is in the synthesis of hierarchical systems and nanowires of ZnO, which has attracted considerable attention due to its potential technological applications attributed to its semiconductor properties.[24,25]

On the other hand, it is well-known that the presence of defects and impurities even at very small concentrations can significantly affect the electrical and optical properties of semiconductors materials.[26,27] In nanowires and hierarchical structures, the large surface area relative to the volume contribute to the increase of defects on their surface, which may act as active sites that are very important for some applications such as photocatalysis and gas sensing enhancement among others.[28−30] Therefore, interpreting the role of defects and impurities is very important to understand the physical properties involved. Local techniques based on hyperfine interactions, where the interaction of the nuclear electromagnetic moments of probe nuclei with the electronic charge and spin distribution in their neighborhood, are useful ways to obtain information related to impurity-host interactions and the presence of defects and dilute clusters in different materials. Among these local techniques are the Mössbauer effect and the perturbed angular correlation (PAC)

spectroscopy, which have been used extensively in condensed matter studies becoming important tools to determine chemical and physical properties within an atomic range.[31,32]

Particularly, PAC spectroscopy is a nonresonance nuclear technique whose signal, therefore, is not affected by high temperatures being capable to measure liquid phases as well. Due to its atomic range and high sensitivity, another great advantage of PAC is its capability of measuring interaction from probe nuclei in different regions throughout the sample. On the other hand, even if the number of isotopes with nuclear properties suitable for PAC experiments is limited this does not prevent the application of the PAC technique to a large variety of studies such as structural and magnetic phase transitions, phase analysis, surface measurements, and interface and grain boundaries and studies of thin films and nanomaterials, diffusion measurements, and thermodynamic properties, among many other properties.[32,33]

In this paper, it is shown that, in order to obtain a simple and inexpensive methodology to grow long ZnO nanowires on oxidized Zn foils, as shown in Scheme 1, the temperature increasing rate plays an important role in the thermal oxidation method. In addition, it is also discussed how a combination of perturbed angular correlation (PAC) spectroscopy, X-ray diffraction (XRD), scanning electron microscopy (SEM), and high-resolution transmission electron microscopy (HRTEM) was essential to quantify and obtain a reasonable interpretation of the thermal oxidation procedure used to produce ZnO with a surface decorated with nanowires starting from a metallic Zn foil. Specifically, PAC measurements could not only identify and quantify a metallic phase trapped inside the ZnO sample, which was not detected by other techniques, but they also determined that this phase was highly oriented.

■ RESULTS AND DISCUSSION

Thermal Oxidation Procedure: Morphology. Figure 1 shows representative SEM images of the Zn foil samples after being submitted to different heating rates. Figure 1a−b displays images of samples that were heated up to 520 °C with a rate of 6 °C/min. A high density of thin ZnO nanowires
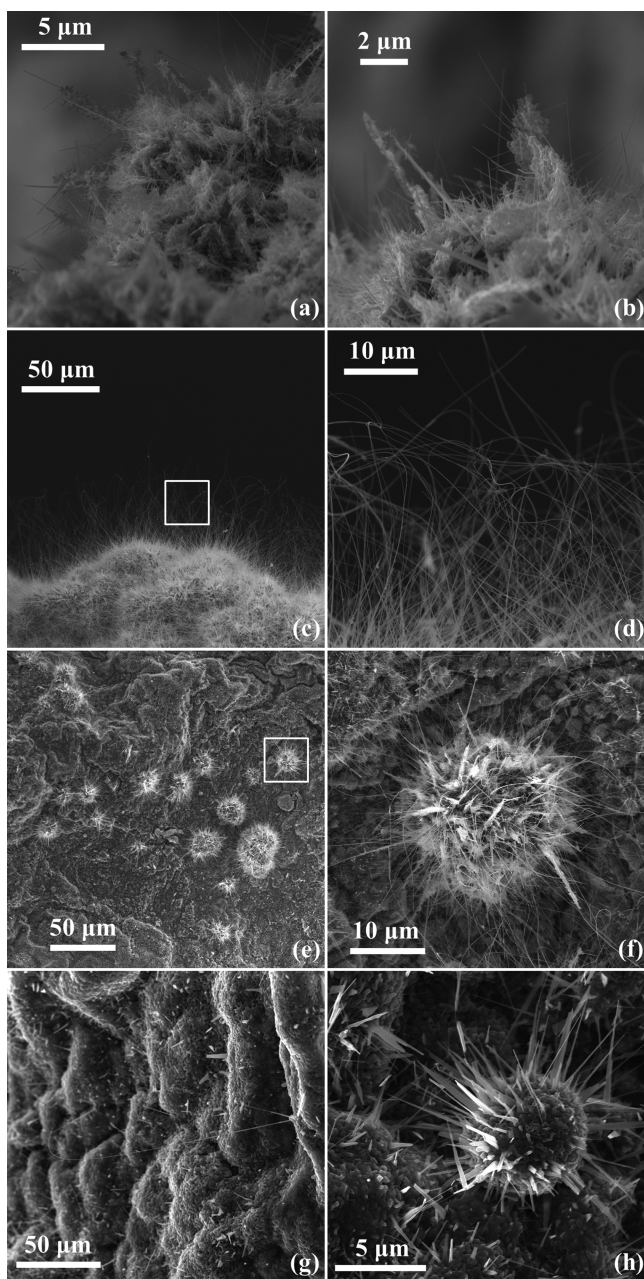
Figure 1. SEM images of zinc oxide wires grown on Zn foils by thermal oxidation at different increasing temperature rates. All samples stayed at maximum temperature for 60 min. Heat treatment at (a–b) 520 °C with a heating rate of 6 °C/min, (c–d) 620 °C with a 20 °C/min rate, (e–f) 620 °C with a 30 °C/min rate, and (g–h) heat treatment at 620 °C with a 50 °C/min rate. A magnified inspection of each samples is shown at the right-hand side.

with length of few μm is clearly seen along with thicker wires. Figure 1c–d shows SEM images of samples oxidized at 620 °C with a heating rate of 20 °C/min. These images display a high population of long (~50 μm) and thin ZnO wires of on the surface of the oxidized Zn foils. It is noteworthy that such thin and long ZnO wires have not been previously observed for this oxidation thermal procedure. In Figure 1e–f, SEM images corresponding to samples submitted to oxidation at 620 °C with a heating rate of 30 °C/min are displayed and show isolated ZnO spheres decorated with ZnO wires with length around 8 μm. Finally, in the SEM images of Figure 1g–h

samples that underwent oxidation at 620 °C, with the heating rate of 50 °C/min display a low density of thicker wires. The inspection on different regions of the sample shown in Figure 1h reveals the formation of isolated ZnO spheres with a diameter greater than 7 μm decorated with nanowhiskers on their surface. The diameter of these nanowhiskers is greater than 200 nm. In addition, all samples submitted to the thermal oxidation procedure remained at maximum temperature for the same reaction time of 60 min, followed by a fast cooling to room temperature. This cooling procedure consists of taking the sample off of the furnace at the maximum temperature and placing it on a ceramic plate to cool down to room temperature.

An additional accurate inspection of the surface of the sample heated at 620 °C with rate 20 °C/min has been carried out in order to obtain details of the long nanowires morphology grown in different regions on it (see Figure 2a–d). It is clearly seen in Figure 2a–b that a high density of long and entangled nanowires with average diameter of 74 nm (see inset in Figure 2d). Insets in Figure 2b–c display junctions of nanowires due to the intercept during the growth process. Transmission electron microscopy (TEM) was used to check the crystallinity of these long nanowires. Images of an isolated nanowire are shown in Figure 2e and g, which allow the determination of the diameter of the three displayed wires (75, 54, and 46 nm are the diameters measured in this sample of nanowires). The high-resolution transmission electron microscopy (HRTEM) image of the top of a typical nanowire is displayed in Figure 2f. The image reveals a periodic atomic arrangement with lattice fringes without fails or piling up, showing the very good crystallinity of ZnO nanowires. In addition, the fast Fourier transform (FFT) patterns of images are shown in Figure 2e and h and, for both, they clearly indicate an hexagonal arrangement that is well oriented along a specific zone axis ($Z = [0001]$). Moreover, the distance between two consecutive lattice planes was determined to be $d = 0.27$ nm. Furthermore, it was also observed that the ZnO nanowires grown along the $\langle 11\bar{2}0 \rangle$ direction. Hence, electron microscopy images reinforce the conclusion that the choice of adequate annealing parameters (temperature, heating rate and reaction time) is very important for the occurrence of long nanowires with good crystallinity grown on the surface of Zn foil by thermal oxidation.

A large number of scientific papers reporting on the growth of ZnO nanowires using different methodologies can be found elsewhere,[16−19] but very few report on the occurrence of long nanowires (above of 10 μm) when the thermal oxidation method is used. As described above, here is presented a methodology to grow long ZnO nanowires on the surface of oxidized Zn foils with the possibility to tune their lengths through the heating rate. In order to check the reproducibility of this method of growing long ZnO nanowires, another sample was prepared following the same thermal heating history of the sample oxidized at 620 °C with a heating rate of 20 °C/min. The resulting SEM images are shown in Figures 1c–d and 2a–d and corroborate the occurrence of long nanowires. We would like to stress that the synthesis of long nanowires has been rarely reported; nevertheless, a few papers emphasize their efficiency in sensorial and photovoltaic applications since a high density of nanowires increases tremendously the active area.[4]

The theoretical description of the growth mechanism of ZnO nanowires using the thermal oxidation method is well
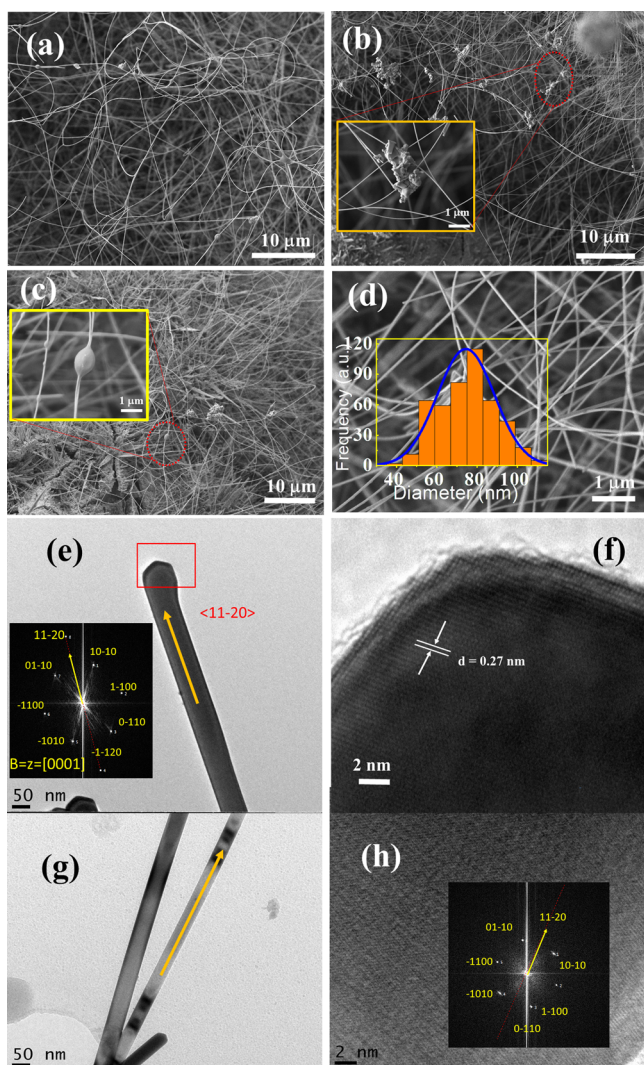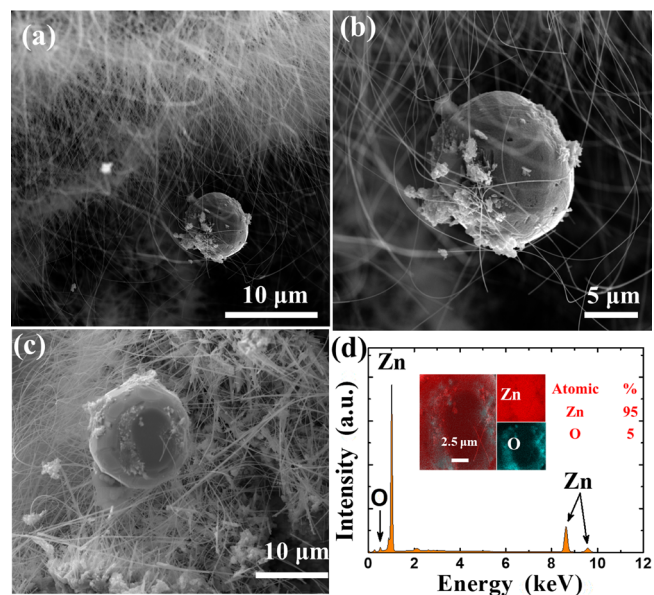
Figure 2. SEM image of different regions of the Zn foil sample heated at 620 °C with rate of 20 °C/min. (a−c) The images reveal a high population of long and entangled nanowires of ZnO, magnified in (d), whose average diameter was determined to be around 74 nm. Insets in (b) and (c) show irregular segregation and junction of nanowires, respectively, due to interception during their growth. (e−h) High-resolution transmission electron microscopy (HRTEM) images of nanowires with the tip of the nanowire shown in e are magnified in f revealing the regular arrangement of lattice fringes. The corresponding fast Fourier transform (FFT) of images are displayed in the insets in (e) and (h), indicating a single-crystal with hexagonal Wurtzite structure with d spacing of around 0.278 nm between neighboring lattice planes along the $\langle 11\bar{2}0 \rangle$ direction.

described, but it is still controversial.[12,13,20,21,24] Results here reported indicate that the growth of ZnO nanowires by he thermal oxidation procedure involves the diffusion of Zn atoms from the Zn−ZnO interface to the surface through the grain boundaries of ZnO layer, usually called the short-circuit/grain boundary diffusion.[16] This process occurs with an anisotropic diffusion of Zn to the external direction, through the surface, energetically favoring the crystalline growth of ZnO. It is noteworthy that, at the interface, the thin ZnO layer, the contribution of oxygen migration is disregarded due to the relatively large atomic size and the high migration energy.[34] The migration energies of interstitial oxygen and oxygen vacancies were reported to be 118 and 124 kJ/mol,

respectively, higher than those for interstitial Zn and Zn vacancies, respectively, 77 and 88 kJ/mol.[12]

In addition, SEM images reveal the presence of small metallic Zn spheres with diameter around 10 μm. These spheres were characterized by EDS spectra and elemental mapping in order to obtain their chemical composition and spatial distribution of the elements present in the spheres. The elemental mapping revealed the presence of Zn in good agreement with results of EDS spectra, as displayed in the inset of Figure 2c. Therefore, these results permit to ensure that the observed droplets are formed by metallic Zn.

The presence of Zn spheres (see Figure 3) and ZnO spheres decorated with nanowires, respectively shown in Figures 4 and

Figure 3. (a) SEM image of different regions of the Zn foil sample heated at 620 °C with a heating rate of 20 °C/min revealing a high population of long nanowires of ZnO. (b) Magnified SEM image focusing on the Zn metal droplet borne by long ZnO nanowires, which shows that the ZnO nanowires have outstanding elastic and plastic properties. (c, d) SEM image, EDS spectrum, and the corresponding EDS elemental mapping of the metallic Zn sphere.

1, is a good indication of the occurrence of flux and diffusion of the liquid metal through possible cracks in the ZnO layer and/or diffusion through grain boundaries due to the hydrostatic stress gradient of liquid Zn. The liquid Zn flow through the ZnO layer favors the formation of Zn spheres, and fast cooling can avoid their full oxidation. On the other hand, with higher heating rates, the oxidation of spheres occurs during the increase in the temperature and the formation of nanowires on their surface follows the same growth mechanism as that for Zn foils. When the sample is cooled down, the spheres are already oxidized. EDS data in Figure 3d confirm that spheres formed during oxidation with 20 °C/min are formed with 95% of Zn with a thin layer of ZnO on the surface, whereas the presence of nanowires in spheres (see Figure 1) formed with higher heating rates is a good indication that they are majorly composed by ZnO.

Therefore, two mechanisms can contribute as driving force to the diffusion and flux of Zn atoms through the ZnO layer, the gradient of hydrostatic stress and the short-circuit diffusion
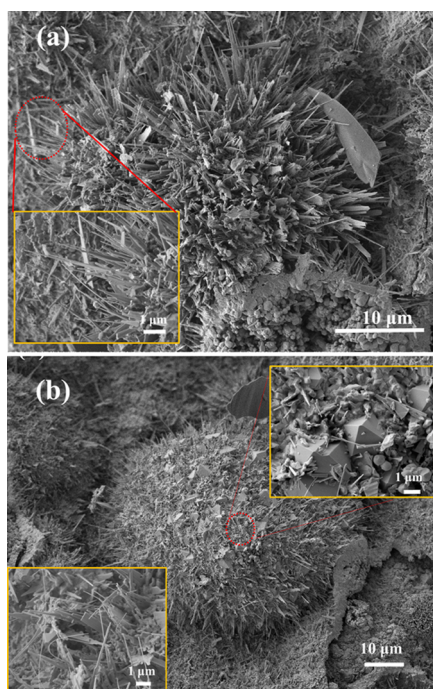
Figure 4. SEM images of different regions of the Zn foil samples oxidized with heating rate of 6 °C/min. (a) Sample heated at 820 °C for 30 min revealing a low density of long ZnO nanowires and nanowhiskers. (inset) 7 μm-long nanowhiskers. (b) Sample heated at 1000 °C for 50 h. (inset) Micrometric ZnO crystals, ZnO nanowires as well as the coalescence between them.

through the grain boundaries or sub-boundaries forming the ZnO nanowires.

It is important to emphasize that the properties of materials at nanoscale have different physical behaviors than those for conventional bulk samples. Among those more affected by the small dimension of the materials are the mechanical properties mainly due to the volume confined in an extremely reduce scale. As reported by Vzinishayan et al.[35] and Agrawal et al.,[36] brittle behavior was observed for the bulk ZnO material whereas the ZnO nanostructures were described to present withstanding large elastic deformation that is dependent on the size of nanowires. Figure 2a−c displays nanowires with diameters around 74 nm bearing solid metallic Zn microspheres with diameters around 12 μm. These images are good representative examples of the elastic and plastic properties of the long ZnO nanowires. As it has been determined by different techniques, such as mechanical resonance experiments and dual-mode resonance, an enhancement of the Young's modulus of ZnO nanowires is related with their diameters. The effective Young's modulus determined using these techniques increased from 140 to 220 GPa as the wire diameter decreased from 120 to 50 nm.[37] After a comparative correlation with the experimental and computational data of Young's modulus reported by Agrawal et al.,[36] the nanowires synthesized in this work with diameters of around 74 nm could then present an estimated Young's modulus of ∼150 GPa. For these reason, the thin and long ZnO nanowires can support an object with higher density such as the metallic Zn spheres with diameter around 12 μm.

In order to investigate the effect of annealing temperature in the formation of nanowires, samples were prepared with heating rate of 6 °C/min and heated with annealing at 820 °C

for 30 min and at 1000 °C for 50 h. SEM images of these samples show the absence of high density of long nanowires but it is possible to observe the presence of ZnO spheres decorated with nanowhiskers in different regions of the samples. These nanowhiskers have lengths around 7 μm as can be seen in the inset of Figure 4a. Interestingly, it is possible to clearly observe the formation of ZnO crystals and the coalescence of wires in the samples annealed at 1000 °C (see inset in Figure 4b). These crystals grow due to the long time of annealing, as expected; on the other side, it is still possible to observe the presence of long and thin nanowires. Samples annealed at 820 °C do not show the presence of crystals only nanowhiskers but with shorter length. The difference in the morphology of these two samples is ascribed to different mechanisms such as the short-circuit diffusion and hydrostatic stress, as already described, for samples annealed at 820 °C, because the annealing temperature is lower than the boiling point (907 °C). For sample annealed at 1000 °C, the annealing temperature is higher than the boiling point, and the presence of Zn vapor could contribute to the occurrence of the observed nanowires while also favoring the coalescence between them (see Figure 4b).

PAC Results. Immediately after diffusion of ^{111}In(^{111}Cd) into the Zn foil, the spin rotation spectrum ($R(t)$) was recorded at room temperature, and it is displayed in Figure 5a. The $R(t)$ spectra were fitted considering all ^{111}Cd probe nuclei experiencing only electric quadrupole interactions characterized by a single and well-defined quadrupole frequency ν_Q = 133.9 (2) MHz with a very small frequency distribution of δ = 0.01 MHz and asymmetry parameter η = 0 corresponding to an axially symmetric local structure. This frequency corresponds to ^{111}Cd probe nuclei replacing crystallographic Zn positions in metallic Zn and, therefore, not occupying interstitial positions. These hyperfine parameter values are in good agreement with those previously reported.[13,38,39] Surprisingly, the shape of the observed spectra is different from that reported for ^{111}Cd at polycrystalline Zn[39] and indicates some degree of texture. This shape is typical of single crystal samples as it is clearly seen in the FFT spectrum (also shown in Figure 5a) in which the intensities of the three frequencies do not follow the 3:2:1 ratio expected for an axially symmetric site of a polycrystalline sample. In order to confirm this observation, another PAC spectrum was acquired with the foil sample lying on the same plane of the detectors (parallel orientation) different from the previous orientation where foil is perpendicular to the detector's plane (perpendicular orientation). A sketch representative of each foil sample orientation with respect to the four detectors' planes is shown in the top panel of Figure 5. The $R(t)$ and FFT spectra obtained after oxidation under different annealing conditions are also shown in Figure 5b−d. The results for $R(t)$ and FFT taken with the parallel orientation displayed in the right side of Figure 5 are quite different from those with the perpendicular orientation at the left side of Figure 5. This strong dependence of $R(t)$ with the preferential orientation is typical of single-crystal samples. The intensities of the transition frequencies ω_n = $g_n(\eta)\nu_Q$ depend on the direction along which the γ rays are detected, with respect to the principal axis system of the electric field gradient (efg) tensor, whose direction is described with reference to the lattice of the host crystal, and therefore, the directions of the γ rays are given with reference to the crystal lattice.[40]
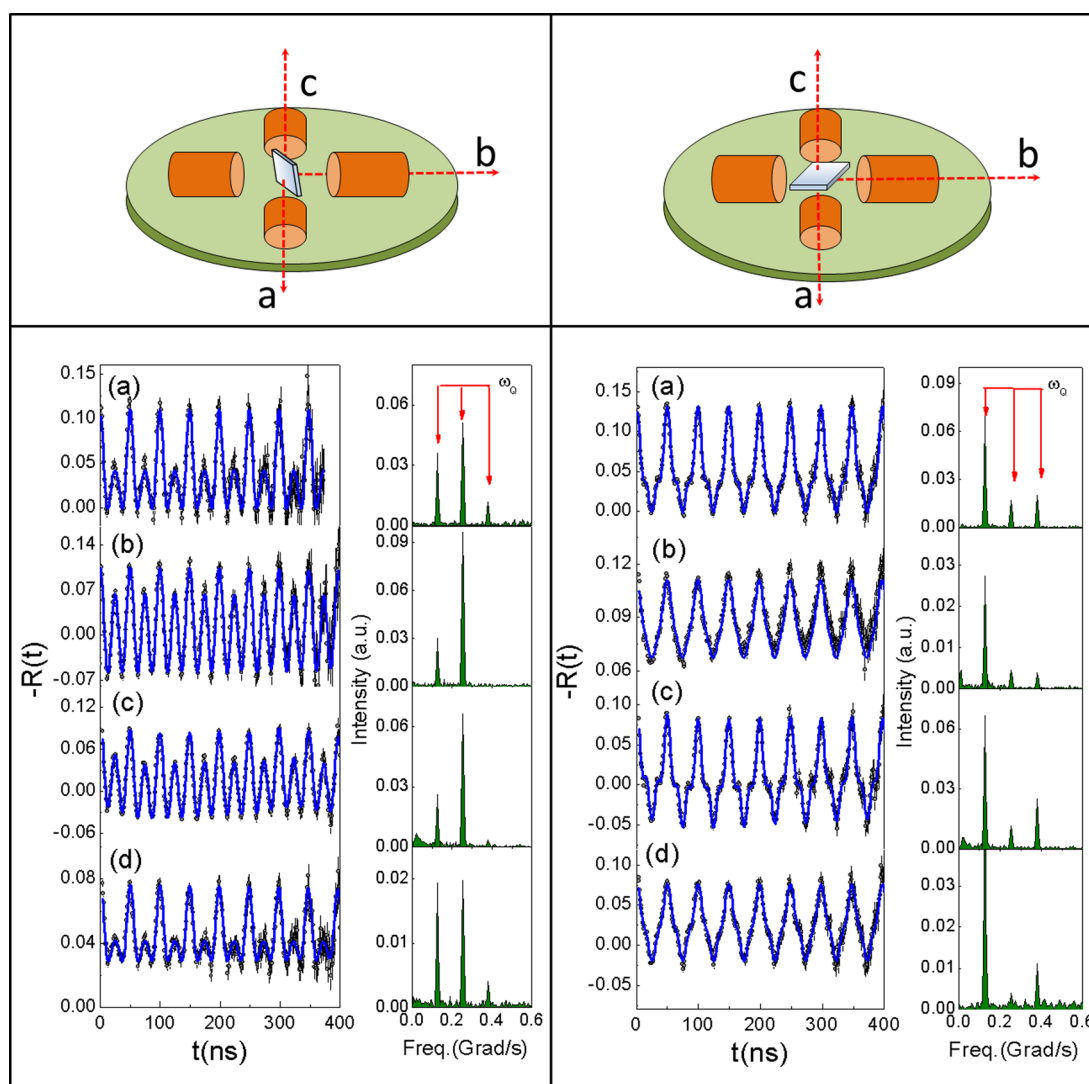
Figure 5. Geometry layout for PAC measurements: perpendicular (left) and parallel (right) orientation of foil relative to the plane of detectors (top panel). Spin rotation $R(t)$ spectra measured with perpendicular (left column) and parallel (right column) orientations along with corresponding FFT spectrum measured with ^{111}In(^{111}Cd) nuclei probe: (a) for metallic Zn after diffusion of ^{111}In at 400 °C during 12 h under He atmosphere. (b) Spin rotation spectra and FFT measured after oxidation at 620 °C (20 °C/min, dwell time of 60 min), (c) 820 °C (6 °C/min, dwell time of 30 min), and (d) 1000 °C (6 °C/min, dwell time of 50 h). Blue solid lines in the spectra represent the least-square fit of the experimental data. All spectra were obtained after fast cooling at room temperature.

PAC measurements were also used to investigate the oxidation process within an atomic range in Zn foil samples submitted to different thermal treatments at high temperatures followed by the fast cooling down to room temperature. After the diffusion of radioactive ^{111}In(^{111}Cd) into the Zn foil samples, they were submitted to the same procedure of thermal oxidation described above. Subsequently after the fast cooling, the spin rotation spectrum for each sample was recorder at room temperature. Figure 5b−d show representative curves of the spin rotation spectra $R(t)$ at perpendicular (left column of Figure 5) and parallel (right column of Figure 5) orientations of the foils at room temperature for samples submitted to thermal heating in air at 620 °C for 60 min, 820 °C for 30 min, and at 1000 °C for 50 h, respectively. The fit of the resulting spectra for sample heated at 620 °C measured in both orientation revealed only quadrupole interactions with single frequency $\nu_Q = 132.6(2)$ MHz and axial symmetry ($\eta = 0$) along the z-axis of the hexagonal crystalline structure of Zn with preferential orientation. All other samples show $R(t)$ spectra with similar parameters also with preferential orientation. The difference in the spectra measured at perpendicular and planar orientations (defining the preferential orientation) are due to the dependence of the efg direction at the probe nucleus site in metallic zinc with respect to the plane of detectors, which is not observed for polycrystalline samples.

Results of XRD measurements for metallic zinc foil show a pattern with typical peaks of the hexagonal structure with space group $P63/mmc$ as displayed in Figure 6a. In addition, Figure 6b displays the representative XRD pattern corresponding to the sample submitted to oxidation at 620 °C obtained after PAC measurements. The analysis indicates the presence of two different crystallographic phases assigned to Zn and ZnO with the $P63/mmc$ and $P63mc$ space group symmetries, respectively. Results show a high intensity peak of Bragg reflection located at $2\theta = 43°$ corresponding to a strong preferential (101) direction indicating a highly textured Zn. These results corroborate the PAC observation of the presence of textured Zn and also confirm the statement that almost all ^{111}Cd nuclei
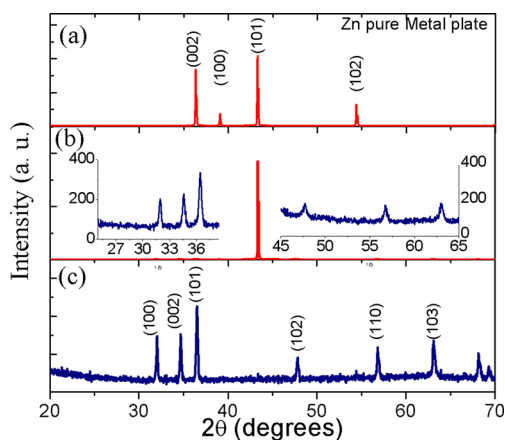
Figure 6. X-ray diffraction patterns for (a) pure metallic Zn foil, (b) Zn foil after thermal oxidation procedure at 620 °C. XRD results show two phases: Zn metal and ZnO. The peak with high intensity was observed due to the (101) preferential orientation. The two insets display the lower intensity peaks of the ZnO. (c) XRD patterns of Zn foil after thermal oxidation procedure at 1000 °C for 50 h, showing a single phase characteristic of the ZnO.

are preferentially replacing metallic Zn rather than Zn sites in ZnO (see Figure 5b). Due to the low intensity of the peaks corresponding to hexagonal wurtzite-type structure of ZnO phase, two enlarged insets were added to Figure 6b in order to display the observed XRD pattern of this phase. Moreover, the XRD pattern of the sample exposed to the high temperature oxidation at 1000 °C for a long time of 50 h is also displayed in Figure 6c. The obtained XRD pattern indicates that the sample crystallize in a single phase corresponding to the ZnO crystal structure. Amazingly, the $R(t)$ spectra for this sample show that probe nuclei populate 100% of a site fraction corresponding to metallic Zn. This observation indicates first, the presence of metallic Zn in the sample, and second, the

preference of ^{111}In(^{111}Cd) to replace Zn sites in metallic Zn instead of ZnO, even when its concentration is extremely small so that XRD is unable to detect it.

Spin-Rotation Spectra at High Temperatures. In order to investigate the behavior of the metallic Zn phase trapped into the samples, as observed by PAC measurements, we have measured PAC spectra of the sample oxidized at 820 °C at different temperatures above the room temperature. XRD results for this sample show similar pattern as that for samples oxidized at 1000 °C, i.e., no peaks for metallic Zn were observed. These measurements were carried out by sealing the samples in quartz tubes under low pressure of helium gas. The ampules containing the sample were placed into a small furnace positioned between the detectors in such a way that the samples were in the parallel position relative to the detector's plane. The spin-rotation spectra were then recorded at different temperatures above room temperature from 25 to 450 °C and are displayed in the left column of Figure 7. The analyses of spectra measured when the temperature increases up to the melting point of Zn ($T_m \sim 420$ °C) were fitted considering pure electric quadrupole interactions for textured or single-crystalline materials (see the left side of Figure 7). The behavior of the temperature dependence of the quadrupole frequency (ν_Q) is such that ν_Q displays slightly decreasing values when temperature increases (see the graph at the bottom of the right side in Figure 7). Similar quadrupole frequency values were reported for PAC measurements on ^{111}Cd in Zn single crystals.[38] However, above the Zn melting point, the $R(t)$ spectra exhibit a large site fraction ($f > 90\%$) characterized by an almost unperturbed quadrupole interaction that is consistent with ^{111}In(^{111}Cd) dissolved in liquid Zn. In addition, PAC results also show that a small population ($f < 10\%$) of probe nuclei can be modeled by a quadrupole interaction with low frequency modulation of around 30 MHz which is characteristic of ^{111}Cd probes which occupy substitutional Zn sites in the ZnO hexagonal structure.[41]
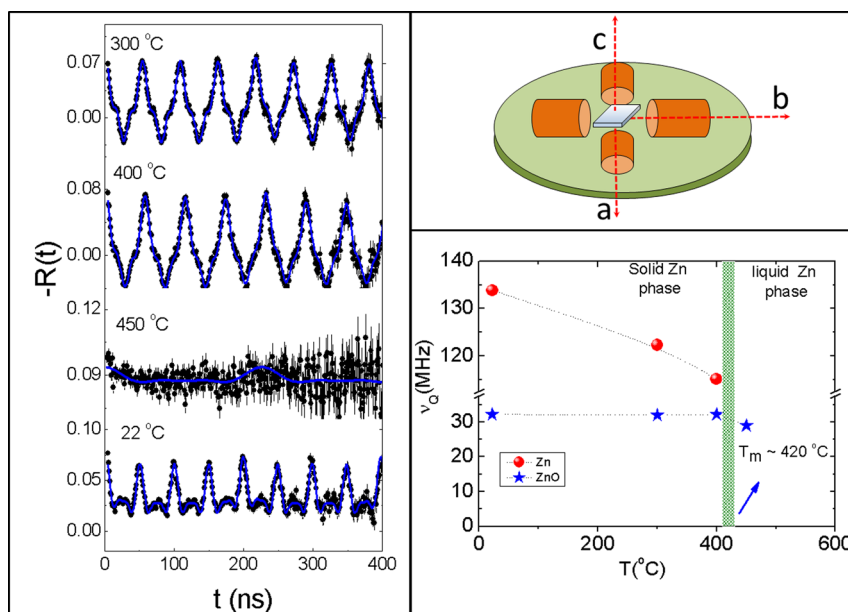
Figure 7. (left) Spin-rotation spectra measured at indicate temperature for sample annealed at 820 °C. The spectrum displayed at the bottom was measured at room temperature after a slow cooling down from 450 °C. The solid lines represent the theoretical fit. (right) The top panel displays a sketch showing the position of the samples in the detector's plane. The bottom panel shows the temperature dependence of the quadrupole frequency (ν_Q) below and above the melting point ($T_m \sim 420$ °C) of Zn metal.
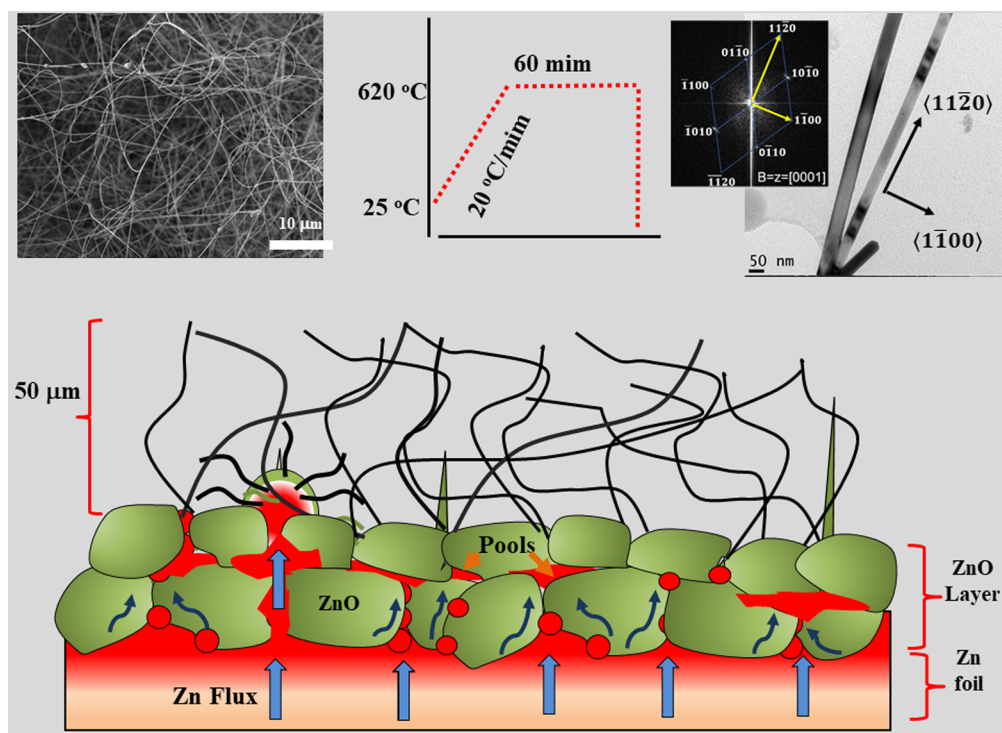
Figure 8. Schematic representation of the oxidized Zn foil with long ZnO nanowires displaying the driving forces of the growth mechanism. Some results concerning the characterization of nanowires are also displayed.

The results indicate the occurrence of interesting phenomena related to the formation of ZnO from the thermal oxidation of Zn. First, a small fraction of the probe nuclei occupy Zn sites at the ZnO crystal structure whereas the major fraction continues to replace Zn sites at the hexagonal structure of the metallic Zn even after oxidation at high temperatures. This observation suggests a higher solubility of indium in metallic Zn even at the liquid phase than in ZnO. A possible mechanism to explain this phenomenon relies on the high jump frequency of indium in metals.[42] As the oxidation process goes forward by diffusion of oxygen into the Zn foil, breaking the metallic bond between Zn atoms, dilute indium atoms jump to the next Zn site in the metallic region not yet oxidized. This process continues until the volume of metallic Zn is too small and the high temperature and pressure drive it through the space between ZnO grains up to the surface. As soon as the Zn reaches the surface, it oxidizes, and due to the gradient of hydrostatic stress, long ZnO nanowires are formed. When the system cools down quickly, the metallic Zn is then trapped in regions between the ZnO grains carrying the majority of the indium atoms with the probe nuclei. Second, the results also show that the probe nuclei in these "pools" of metallic Zn trapped between the grains of ZnO sense quadrupole interactions typical of textured materials with a preferential direction. The same phenomenon was observed in ZnO microtubes decorated with shorter nanowires and reported by Rivaldo-Gómez et al.[13] The work reported by Yin et al. describes a similar situation for ^{111}In(^{111}Cd) in metallic gallium.[43,44]

Since XRD measurements do not reveal the presence of Zn, the occurrence of metallic Zn observed by PAC, which certainly has an influence on transport properties, may be in the form of very thin layers trapped between ZnO grains. The difference in detecting the metallic Zn between both

techniques can be ascribed to the local character of PAC that is able to observe the environment around the probe nuclei within an atomic range. In addition, the preference of In for Zn instead of ZnO can also indicate that thermal oxidation would not a good technique to synthesize oxide heterostructures from doped metals, at least for Zn doped with In.

On the other hand, after PAC measurements at 450 °C, the sample was slowly cooled down to room temperature (cooling time of 120 min) and had the spin-rotation spectrum recorded. The results show a quite different $R(t)$ spectrum, however, with the same quadrupole frequency but with a spectrum modulation that is characteristic of the polycrystalline Zn metal and does not show the textured behavior observed before. Consequently, these results indicate that the occurrence of the highly textured "pools" of metallic Zn is related to the rate of the cooling process. The presence of very small textured metallic Zinc regions trapped inside the ZnO layers is essential to some important physical behaviors related, for instance, to electric, optical, and sensory properties of the substrates decorated with long entangled nanowires. Therefore, metallic regions inside low-dimension semiconductor oxides such as ZnO foils, which certainly affect its transport properties, can trigger a new unexplored research field on these materials aiming to improve physical and chemical properties useful for interesting technological applications.

The schematic representation in Figure 8 summarizes the diffusion mechanisms that favor the formation of the ZnO layer decorated by long nanowires during the thermal oxidation of Zn foils. One of these mechanisms is the short circuit diffusion, which consist of the energetically favored anisotropic diffusion of Zn atoms from the foil toward the surface inducing the growth of crystalline ZnO layer. As can be seen in the scheme, the ZnO layer has a fundamental role in the growth of nanowires since it regulates the diffusion of Zn

and O atoms as well as vacancies that are kinetically stimulated in the oxidation process. In addition, in the ZnO layer, grain boundaries and displacements are formed where the nucleation of nanowires or whiskers takes place and act as diffusion tracks for the oriented growth of nanowires. After nucleation, the growth of nanowires depends on the mobility of interstitial Zn that follows an oriented direction which, in the present work, is $\langle 11\bar{2}0 \rangle$. During the temperature increase after melting at 420 °C, liquid Zn significantly increases in volume to a hydrostatic pressure due to the confinement of this liquid by the ZnO layer. According to the work of Chen et al.,[14] the gradient of hydrostatic stress acts as a driving force for atomic diffusion and the atomic flux is in the direction from the more compressive to less compressive region. This Zn flux flows through tracks between the grain boundaries; also, the flux pressure can form cracks in the ZnO layer reaching the surface and forming the nanowires. With the increase in the temperature, the hydrostatic pressure increases widening the cracks and inducing the formation of thicker nanowires or whiskers. When the sample is cooled down quickly, Zn liquid regions solidify with preferred orientation. Conversely, when the cooling of samples is slow, the orientation is isotropic. This method has been used to grow nanowires of aluminum[46] and CuO.[47]

■ EXPERIMENTAL SECTION

Synthesis of Long ZnO Nanowires. The synthesis of the ZnO nanowires is started by using a high purity Zn metal (99.9999%) in the form of a thick foil. Initially, metal samples were submitted to a cleaning process with isopropyl alcohol in an ultrasonic bath and subsequently dried in a desiccator at low pressure using a vacuum pump. Immediately after cleaning, samples were placed in alumina crucibles to perform the thermal oxidation under air at room pressure. As already reported, a good size and high density of the ZnO nanowires were achieved between 500 and 700 °C.[16] In the present work, in order to obtain the best description of the oxidizing procedure of the Zn foils, a systematic study was performed as a function of the heating rate up to a specific temperature (dwell temperature) and also as a function of the annealing at this dwell temperature. First, the Zn foils were oxidized with a heating rate of 6 °C/min up to 520 °C, and this temperature was held for 60 min. Subsequently, samples were removed from the furnace and immediately laid on a ceramic plate to cool down rapidly to room temperature; a procedure here called "fast cooling". Second, samples were heated up to 620 °C with different heating rates of 20, 40, and 50 °C/min, maintaining the reaction time of 60 min. After this procedure, samples were fast cooled to room temperature. During the oxidizing reaction at the dwell temperature, a thin ZnO layer is formed on the surface of foils preserving the shape of the substrate. This thin layer is responsible for controlling the exchange diffusion of the Zn−O atoms, i.e., the outward diffusion of the Zn atom and the inward diffusion of oxygen into the ZnO/Zn substrate. In general, metal ions (like Zn) often diffuse outward faster than oxygen ions diffuse inward through the grain boundaries and interstitials, a procedure called short-circuit diffusion. These mechanisms can be described by mass transport in which the temperature rate plays an important role to determine the morphology and the growth of the nanowires on the substrate. After oxidation, in order to obtain a morphological and crystalline characterization, the samples were inspected by scanning electron microscopy (SEM), high-resolution transmission electron microscopy (HRTEM), and energy dispersive X-ray spectroscopy (EDS).

Local Inspection of Thermal Oxidation Procedure: PAC Measurements. In order to observe the samples from a local view, a nuclear technique with resolution of atomic distances has been used. The perturbed angular correlations (PAC) technique measures hyperfine interactions between the extra nuclear magnetic hyperfine

field (B_{hf}) and/or the electric field gradient (efg) tensor with the nuclear moments of a certain probe nucleus. This method uses radioactive probe nuclei for measurements, and in this work, we used ^{111}Cd as the probe nuclei replacing Zn lattice positions. ^{111}Cd results from the electron-capture decay of the parent nucleus ^{111}In; therefore, hereafter it will be represented as ^{111}In(^{111}Cd). Results from PAC experiments are the spin-rotation spectra $R(t) = A_{22} \sum_i f_i G_{22}^i(t)$, fitted by a model that takes into account the fractional site population (f) of probe nuclei and their respective perturbation function $G_{22}(t)$. A_{22} is the angular correlation coefficient, which, for ^{111}In(^{111}Cd), $A_{22} = -0.18$,[45] and because it is negative, the spin-rotation spectra are displayed as $-R(t)$ with the y axis inverted. For magnetic hyperfine interactions, $G_{22}(t) = 0.2 + 0.4 \sum_{n=1,2} \cos(n\omega_L t)$, and its measurement allows the determination of the Larmor frequency $\omega_L = \mu_N g B_{hf}/\hbar$, where μ_N is the nuclear magnetron and g is the nuclear g-factor, and the calculation of the magnetic hyperfine field B_{hf}. The perturbation function for electric quadrupole interactions is given by $G_{22}(t) = S_{20} + \sum_{n=1,2,3} S_{2n}(\eta) \cos(\omega_n t)$, where the transition frequencies $\omega_n = g_n(\eta)\nu_Q$ are proportional to the quadrupole frequency $\nu_Q = eQV_{zz}/h$, and, as well as the S_{2n} coefficients, depend on the asymmetry parameter $\eta = (V_{xx} - V_{yy})/V_{zz}$. The quadrupole frequency ν_Q and η can be then experimentally determined allowing the calculation of the V_{kk}, $k = x, y, z$, components of the electric field gradient tensor.

PAC measurements were carried out at IPEN using ^{111}Cd as the probe nucleus, which is produced from the decay of the radioactive ^{111}In by the electron capture process (EC-decay) that leaves the ^{111}Cd in an excited state. The decay of ^{111}Cd to the ground state occurs by the emission of two successive gamma-rays (171 and 245 keV) The ^{111}In nuclei were introduced into the Zn foils by thermal diffusion (in concentrations well below 1 ppm). A volume containing approximately 100 μCi of ^{111}InCl$_3$ solution was dropped on the surface of three Zn metallic foils, which were subsequently encapsulated into quartz tubes under low pressure of helium atmosphere to avoid the metal oxidation during the diffusion of the radioactive nuclei probe performed at 400 °C during 12 h followed by a fast cooling. This temperature has been chosen in order to preserve the shape of the metal foils as well as to avoid the formation of the liquid phase of Zn. After diffusion of probe nuclei, three samples were oxidized in air heated at 20 °C/min up to 620 °C (dwell time of 60 min), at 5 °C/min up to 820 °C (dwell time of 30 min), and at 5 °C/min up to 820 and 1000 °C (dwell time of 50 h), fast cooled, and measured at room temperature. The resulting spin rotation spectra, $R(t)$, from the PAC measurements were modeled taking into account only electric quadrupole interactions. After the radioactivity decay of ^{111}In(^{111}Cd) probes diffused into the studied samples, these had their crystalline structure characterized by XRD using a Bruker D8-ADVANCE.

■ CONCLUSIONS

In the work here reported, long ZnO nanowires were grown on the surface of zinc oxide obtained by thermal oxidation of the Zn foil. Particularly, samples submitted to thermal oxidation at 620 °C, with a heating rate of 20 °C/min revealed the growth of long ZnO nanowires, with a length of around 50 μm and diameter of ∼74 nm with a high population density as confirmed by scanning electron microscopy and high-resolution transmission electron microscopy which also revealed the regular atomic arrangement of lattice fringes without any stacking faults and dislocations, indicating an excellent crystallinity of ZnO nanowires grown along the $\langle 11\bar{2}0 \rangle$ direction.

The results indicate that the growth of long ZnO nanowires is induced by two mechanisms that contribute as driving forces to the diffusion and flux of Zn atoms through the ZnO layer, the gradient of hydrostatic stress, and the short-circuit diffusion through the grain boundaries or sub-boundaries forming the ZnO nanowires. Oxygen diffusion migration is disregarded due to the relatively large atomic size and the higher migration

energy when compared to that of Zn diffusion. Moreover, for these samples, X-ray diffraction and perturbed angular correlations (PAC) reveal the presence of high texture with preferential crystalline orientation of metallic Zn still present in the samples.

For samples submitted to thermal oxidation at high temperatures, although XRD shows only the presence of ZnO and does not show any peak of the metallic Zn phase, PAC measurements reveal a major fraction (>90%) of probe nuclei at the metallic phase with a textured pattern. These results clearly show the preference of In atoms for metallic Zn and the presence of very small thin regions ("pools") of this phase trapped between the ZnO grains and that they are also a clue for the growth of long ZnO nanowires decorating the surface of the oxidized foil. Moreover, results also confirm that the diffusion of Zn through grain border of ZnO is the main driving force for the growth of ZnO nanowires on the surface and suggest the possible mechanism for this diffusion would be the short-circuit diffusion and the gradient of hydrostatic stress. The texture of metallic zinc present in the form of thin films in ZnO is very important to electric, optical, and sensorial proprieties. Finally, the PAC results also shed light on the difference of solubility of In in Zn and ZnO revealing that In has a high preference for Zn which indicates that thermal oxidation would not be a good technique for the formation of oxides from doped metals and opening a possible research area in hierarchical semiconductor oxides doped with metal or on metallic alloys in semiconductor materials. Lastly, due to the extremely large surface area, high-density ZnO nanowires grown on ZnO surfaces with thin metallic Zn regions are very good candidates for high-efficiency microgas sensors.

■ AUTHOR INFORMATION

Corresponding Author
*E-mail: carbonar@ipen.br. Phone: +55(11)31338807.
ORCID ⊙
A. W. Carbonari: 0000-0002-4499-5949

Notes
The authors declare no competing financial interest.

■ ACKNOWLEDGMENTS

■ REFERENCES

(1) Suh, Y. D.; Hong, S.; Kim, G.; Hwang, K.-I.; Choi, J.-H.; Hong, W.-H.; Yeo, J.; Ko, S. H. Selective Electro - Thermal Growth of Zinc Oxide Nanowire on Photolithographically Patterned Electrode for Microsensor Applications. *Int. J. Precision Engineering and Manufacturing-Green Technology* **2016**, *3*, 173−177.

(2) Ma, C.-W.; Chang, C.-M.; Huang, P.-C.; Yang, Y.-J. Sea-Urchin-Like ZnO Nanoparticle Film for Dye-Sensitized Solar Cells. *J. Nanomater.* **2015**, *2015*, 679474.

(3) Bagga, S.; Akhtar, J.; Mishra, S. Synthesis and applications of ZnO nanowire: A review. *AIP Conf. Proc.* **2017**, *1989*, 020004.

(4) Ko, S. H.; Lee, D.; Kang, H. W.; Nam, K. H.; Yeo, J. Y.; Hong, S. J.; Grigoropou-los, C. P.; Sung, H. J. Nanoforest of Hydrothermally Grown Hierarchical ZnO Nanowires for a High Efficiency Dye-Sensitized Solar Cell. *Nano Lett.* **2011**, *11*, 666−671.

(5) Tian, Z. R.; Voigt, J. A.; Liu, J.; Mckenzie, B.; Mcdermott, M. J.; Rodriguez, M. A.; Konishi, H.; Xu, H. Complex and oriented ZnO nanostructures. *Nat. Mater.* **2003**, *2*, 821−826.

(6) Chauvin, A.; Delacôte, C.; Boujtita, M.; Angleraud, B.; Ding, J.; Choi, C.-H.; Tessier, P.-Y.; El Mel, A.-A. Dealloying of gold-copper alloy nanowires: From hillocks to ring-shaped nanopores. *Beilstein J. Nanotechnol.* **2016**, *7*, 1361−1367.

(7) Lee, Y. J.; Lee, Y.; Oh, D.; Chen, T.; Ceder, G.; Belcher, A. M. Biologically Activated Noble Metal Alloys at the Nanoscale: For Lithium Ion Battery Anodes. *Nano Lett.* **2010**, *10*, 2433−2440.

(8) Amato, M.; Palummo, M.; Rurali, R.; Ossicini, S. Silicon-Germanium Nanowires: Chemistry and Physics in Play, from Basic Principles to Advanced Applications. *Chem. Rev.* **2014**, *114*, 1371−1412.

(9) Ambrosini, S.; Fanetti, M.; Grillo, V.; Franciosi, A.; Rubini, S. Vapor-liquid-solid and vapor-solid growth of self-catalyzed GaAs nanowires. *AIP Adv.* **2011**, *1*, 042142.

(10) Wu, Z. H.; Mei, X. Y.; Kim, D.; Blumin, M.; Ruda, H. E. Growth of Au-catalyzed ordered GaAs nanowire arrays by molecular-beam epitaxy. *Appl. Phys. Lett.* **2002**, *81*, 5177−5179.

(11) Jang, S. Y.; Song, Y. M.; Kim, H. S.; Cho, Y. J.; Seo, Y. S.; Jung, G. B.; Lee, C.-W.; Park, J.; Jung, M.; Kim, J.; Kim, B.; Kim, J.-G.; Kim, Y.-J. Three Synthetic Routes to Single-Crystalline PbS Nanowires with Controlled Growth Direction and Their Electrical Transport Properties. *ACS Nano* **2010**, *4*, 2391−2401.

(12) Rackauskas, S.; Nasibulin, A. G.; Jiang, H.; Tian, Y.; Statkute, G.; Shandakov, S. D.; Lipsanen, H.; Kauppinen, E. I. Mechanistic investigation of ZnO nanowire growth. *Appl. Phys. Lett.* **2009**, *95*, 183114.

(13) Rivaldo-Gómez, C. M.; Cabrera-Pasca, G. A.; Zuniga, A.; Carbonari, A. W.; Souza, J. A. Hierarchically structured nanowires on and nanosticks in ZnO microtubes. *Sci. Rep.* **2015**, *5*, 15128.

(14) Chen, M.; Yue, Y.; Ju, Y. Growth of metal and metal oxide nanowires driven by the stress-induced migration. *J. Appl. Phys.* **2012**, *111*, 104305.

(15) Nasibulin, A. G.; Rackauskas, S.; Jiang, H.; Tian, Y.; Mudimela, P. R.; Shandakov, S. D.; Nasibulina, L. I.; Jani, S.; Kauppinen, E. I. Simple and rapid synthesis of a-Fe₂O₃ nanowires under ambient conditions. *Nano Res.* **2009**, *2*, 373−379.

(16) Shih, P.-H.; Wu, S. Y. Growth Mechanism Studies of ZnO Nanowires: Experimental Observations and Short-Circuit Diffusion Analysis. *Nanomaterials* **2017**, *7*, 188.

(17) Hirate, T.; Sasaki, S.; Li, W.; Miyashita, H.; Kimpara, T.; Satoh, T. Effects of laser-ablated impurity on aligned ZnO nanorods grown by chemical vapor deposition. *Thin Solid Films* **2005**, *487*, 35−39.

(18) Wagner, R. S.; Ellis, W. C. Vapor-Liquid-Solid Mechanism of Single Crystal Growth. *Appl. Phys. Lett.* **1964**, *4*, 89−90.

(19) Sun, Y.; Fuge, G. M.; Ashfold, M. N. R. Growth of aligned ZnO nanorod arrays by catalyst-free pulsed laser deposition methods. *Chem. Phys. Lett.* **2004**, *396*, 21−26.

(20) Choopun, S.; Hongsith, N.; Wongrat, E. Metal-Oxide Nanowires by Thermal Oxidation Reaction Technique. In *Nanowires*; Prete, P., Ed.; Intechopen Ld.: London, United Kingdom, 2010; pp 97−115.

(21) Yuan, L.; Wang, Y.; Mema, R.; Zhou, G. Driving force and growth mechanism for spontaneous oxide nanowire formation during the thermal oxidation of metals. *Acta Mater.* **2011**, *59*, 2491−2500.

(22) Zhao, C. X.; Li, Y. F.; Zhou, J.; Li, L. Y.; Deng, S. Z.; Xu, N. S.; Chen, J. Large-Scale Synthesis of Bicrystalline ZnO Nanowire Arrays by Thermal Oxidation of Zinc Film: Growth Mechanism and High-Performance Field Emission. *Cryst. Growth Des.* **2013**, *13*, 2897−2905.

(23) Lin, Z.; Zhao, P.; Ye, P.; Chen, Y.; Gan, H.; She, J.; Deng, S.; Xu, N.; Chen, J. Maximum field emission current density of CuO nanowires: theoretical study using a defect-related semiconductor field emission model and in situ measurements. *Sci. Rep.* **2018**, *8*, 2131.

(24) Xu, S.; Wang, Z. L. One-dimensional ZnO nanostructures: Solution growth and functional properties. *Nano Res.* **2011**, *4*, 1013−1098.

(25) Wongrat, E.; Pimpang, P.; Choopun, S. Comparative study of ethanol sensor based on gold nanoparticles: ZnO nanostructure and gold: ZnO nanostructure. *Appl. Surf. Sci.* **2009**, *256*, 968−971.

(26) Ahn, M.-W.; Park, K.-S.; Heo, J.-H.; Park, J.-G.; Kim, D.-W.; Choi, K. J.; Lee, J.-H.; Hong, S.-H. Gas sensing properties of defect-controlled ZnO-nanowire gas sensor. *Appl. Phys. Lett.* **2008**, *93*, 263103.

(27) Yang, X.; Wolcott, A.; Wang, G.; Sobo, A.; Fitzmorris, R. C.; Qian, F.; Zhang, J. Z.; Li, Y. Nitrogen-Doped ZnO Nanowire Arrays for Photoelectrochemical Water Splitting. *Nano Lett.* **2009**, *9*, 2331−2336.

(28) Dietl, T. A ten-year perspective on dilute magnetic semiconductors and oxides. *Nat. Mater.* **2010**, *9*, 965−974.

(29) Ohno, H. Making Nonmagnetic Semiconductors Ferromagnetic. *Science* **1998**, *281*, 951−956.

(30) Ohno, H. A window on the future of spintronics. *Nat. Mater.* **2010**, *9*, 952−954.

(31) Yoshida, Y.; Langouche, G. Nuclear Methods to Study Defects and Impurities in Si Materials. In *Defects and Impurities in Silicon Materias: An Introduction to Atomic-Level Silicon Engineering*; Yoshida, Y., Langouche, G., Eds.; Springer: Tokyo, 2015; pp 375−429.

(32) Schatz, G.; Weidinger, A. *Nuclear condensed matter physics: Nuclear methods and applications*, 2nd ed.; J. Wiley and Sons: Chichester, United Kingdom, 1996; pp 63−99.

(33) Carbonari, A. W.; Mestnik-Filho, J.; Saxena, R. N. Impurities in Magnetic Materials Studied by PAC Spectroscopy. *Defect Diffus. Forum* **2011**, *311*, 39−61.

(34) Ren, S.; Bai, Y. F.; Chen, J.; Deng, S. Z.; Xu, N. S.; Wu, Q. B.; Yang, S. Catalyst-free synthesis of ZnO nanowire arrays on zinc substrate by low temperature thermal oxidation. *Mater. Lett.* **2007**, *61*, 666−670.

(35) Vazinishayan, A.; Yang, S.; Lambada, D. R.; Wang, Y. Mechanical behavior enhancement of ZnO nanowire by embedding different nanowires. *Results Phys.* **2018**, *9*, 218−224.

(36) Agrawal, R.; Peng, B.; Gdoutos, E. E.; Espinosa, H. D. Elasticity Size Effects in ZnO Nanowires-A Combined Experimental-Computational Approach. *Nano Lett.* **2008**, *8*, 3668−3674.

(37) Hoffmann, S.; Östlund, F.; Michler, J.; Fan, H. J.; Zacharias, M.; Christiansen, S. H.; Ballif, C. Fracture strength and Young's modulus of ZnO nanowires. *Nanotechnology* **2007**, *18*, 205503.

(38) Meyer, F.; Deubler, S.; Plank, H.; Witthuhn, W.; Wolf, H. Grain size dependence of the electric field gradient. *Hyperfine Interact.* **1987**, *34*, 243−246.

(39) Raghavan, P.; Raghavan, R. S.; Kaufmann, E. N.; Krien, K.; Naumann, R. A. Nuclear quadrupole interaction of ^{111}Cd in zinc (by PAC). *J. Phys. F: Met. Phys.* **1974**, *4*, L80−L83.

(40) Wichert, T.; Deicher, M.; Grübel, G.; Keller, R.; Schulz, N.; Skudlik, H. Indium-defect complexes in silicon studied by perturbed angular correlation spectroscopy. *Appl. Phys. A: Solids Surf.* **1989**, *48*, 59−85.

(41) Mercurio, M.E.; Carbonari, A.W.; Cordeiro, M.R.; Saxena, R.N.; D'Agostino, L.Z. Local investigation of hyperfine interactions in pure and Co-doped ZnO. *J. Magn. Magn. Mater.* **2010**, *322*, 1195−1197.

(42) Collins, G. S.; Jiang, X.; Bevington, J. P.; Selim, F.; Zacate, M. O. Change of Diffusion Mechanism with Lattice Parameter in the Series of Lanthanide Indides Having L1$_2$ Structure. *Phys. Rev. Lett.* **2009**, *102*, 155901.

(43) Yin, X. Y.; Collins, G. S. The Solubility of Indium in Liquid Gallium Supercooled to 12 K. *Defect Diffus. Forum* **2012**, *323−325*, 503−508.

(44) Newhouse, R.; Collins, G. S.; Zacate, M. O. Site occupation of indium and jump frequencies of cadmium in FeGa$_3$. *Hyperfine Interact.* **2016**, *237*, 137.

(45) Rinneberg, H. H. Application of perturbed angular correlation to chemistry and related areas of solid state physics. *At. Energy Rev.* **1979**, *17*, 477−595.

(46) Lee, H. T.; Kimura, Y.; Saka, M. Fabrication of aluminum microwires through artificial weak spots in a thick film using stress-induced migration. *AIMS Materials Science* **2018**, *5*, 591−602.

(47) Yue, Y.; Chen, M.; Ju, Y.; Zhang, L. Stress-induced growth of well-aligned Cu$_2$O nanowire arrays and their photovoltaic effect. *Scr. Mater.* **2012**, *66*, 81−84.